Journal of Energy and Power Engineering 11 (2017) 605-613
doi: 10.17265/1934-8975/2017.09.006

Fundamental Study of High Step-down Non-isolated Multicellular DC-DC Converter for Future DC Distribution Systems

Yusuke Hayashi, Yoshikatsu Matsugaki and Tamotsu Ninomiya
Green Electronics Research Institute, Kitakyusyu, Fukuoka 808-0135, Japan

Received: August 08, 2017 / Accepted: August 16, 2017 / Published: September 30, 2017

Abstract: A novel high step-down non-isolated DC-DC converter has been proposed. The proposed converter consists of highly efficient non-isolated cell converters using bidirectional semiconductor power devices, and these cell converters are connected in ISOP (input series and output parallel). The non-isolated ISOP converter achieves high step-down ratio of *D*/N, operating N cell converters under the duty ratio of *D*. Availability of the proposed converter has been shown by developing the 48 V-12 V laboratory prototype using two 24 V-12 V cell converters. Design consideration for the 48 V-3 V multicellular converter using four 12 V-3 V cell converters has been also conducted, and the potential to approach the efficiency of 97% has been discussed. The proposed topology is suitable for the POL (point of load) converters in the highly efficient next generation DC distribution system for data centers.

Key words: DC-DC converter, high step-down ratio, ISOP, GaN (gallium nitride).

1. Introduction

The amount of the network traffic in data centres has been rapidly increasing due to the widespread use of the ICT (information and communication technology) equipment [1, 2]. The energy and the resource savings in data centres will contribute to solving some of our global environmental problems. The NTT (Nippon Telegraph and Telephone) group has been proposing the next generation environmentally friendly DC distribution system to realize highly electrified future low-carbon societies [3-5].

Highly efficient and ultra-compact (high power density) power converters are indispensable to develop the next generation dc distribution system shown in Fig. 1 [4]. The PFC (power factor correction) converter with the efficiency of 99% and the DC-DC transformer with the efficiency of 98% have been already reported [6, 7]. Highly efficient and high step-down POL (point-of-load) converters are necessary for the DC distribution system.

The magnetic coupling such as the transformers and the coupled inductors are generally applied to develop the high step-down POL converters [8-10]. The performance of the high step-down converter largely depends on the characteristics of the magnetic material. The progress of the magnetic component determined by the material science is one of barriers to achieve future high power density converters [11].

The high step-down non-isolated DC-DC converter based on the multicellular converter topology is newly proposed here. The proposed converter consists of low-voltage and low-power cell converters using bidirectional semiconductor devices, and the cell converters are connected in ISOP (input series output parallel). One of features of the proposed converter is the lower stress for the magnetic components. The

Corresponding author: Yusuke Hayashi, Dr. Eng., research fields: DC distribution system, DC power supply and power electronics system integration.

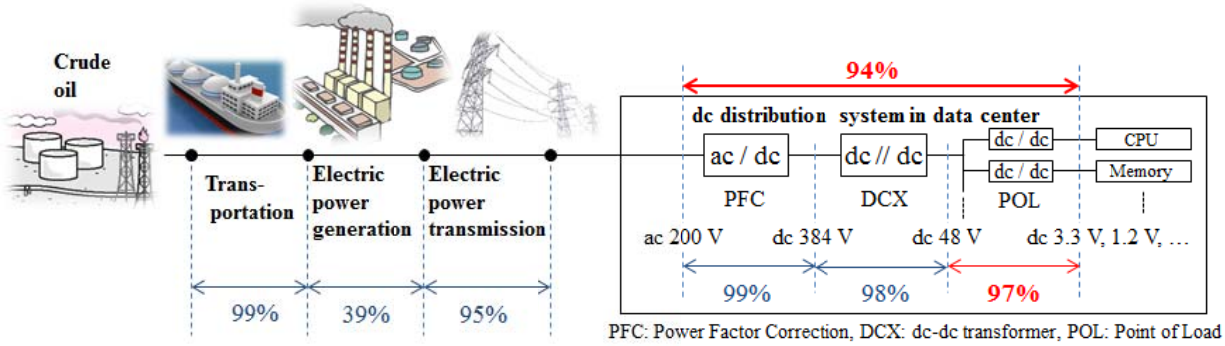

Fig. 1 Configuration of next generation dc distribution system for environmentally friendly data centers.

magnetic coupling is not applied in the proposed converter, and the stored energy in the inductors can be reduced by the interleaved control of the cell converters. In Section 2, the high step-down non-isolated DC-DC converter is introduced. The circuit configuration, the control method and the characteristics are shown here. In Section 3, the feasibility of the proposed converter is shown by fabricating the breadboard of 48 V-12 V multicellular converter using two 24 V-12 V cell converters. In the Section 4, the design consideration for the 48 V-3 V multicellular converter is carried out and the future prospect is discussed.

2. High Step-down Non-isolated Multicellular DC-DC Converter

2.1 High Step-down DC-DC Converter Based on Magnetic Coupling Topology

The step-down ratio (the input voltage/the output voltage) of the POL converter is e.g. 14.5 (= 48/3.3) or 40 (= 48/1.2) in the DC distribution system shown in Fig. 1. In the case of the general buck chopper circuit, the duty ratio of the main switch is calculated at 0.069 (= 1/14.5) or 0.025 (1/40). High-speed and ultra-low loss semiconductor power devices are indispensable to achieve the buck chopper operation under the extremely low duty ratio control. The buck converter with the efficiency of 80% to 86% using GaN-FETs has been reported for the single high-ratio step-down converter system [12].

The isolated DC-DC converter is one of solutions for the high step-down voltage transformation ratio. The turn ratio of the primary and the secondary windings of the high frequency transformer achieve the high voltage transformation ratio easily, and the high efficiency is accomplished by the soft-switching technology for the power devices. Highly efficient and ultra-compact magnetically coupled power converters over 90% have been reported in Refs. [8, 13].

The multicellular converter topology is also one of options to realize the high step-down DC-DC converter. The multicellular topology means the building block of the low-voltage, low-power cell converters. The power converters with low-voltage transformation ratio are available for the cell converters, and the possibility of the converter design can be expanded.

The conceptual diagram of the multicellular DC-DC converter is shown in Fig. 2. The multicellular converter

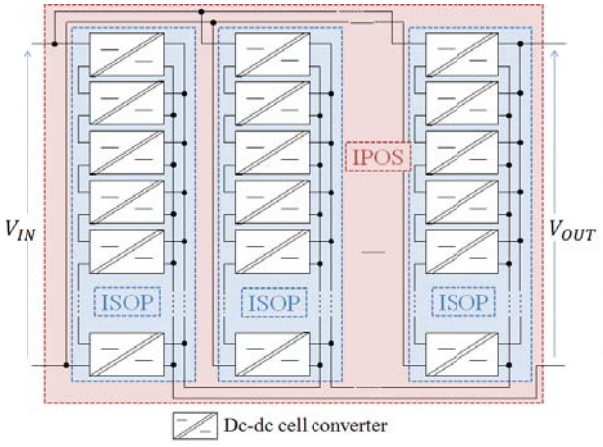

Fig. 2 Conceptual diagram of multicellular DC-DC converter based on ISOP-IPOS circuit topology.

consists of a lot of standardized, low-voltage isolated DC-DC cell converters mainly. These cell converters are connected in ISOP to achieve the high step-down voltage transformation ratio, and cell converters are connected in IPOS (input parallel output series) to achieve the high step-up transformation ratio. Features of the multicellular DC-DC converter are summarized as follows.

- The efficiency η (%) and the power density D_p (W/cm^3) of the multicellular DC-DC converter corresponds to the performances of the single cell converter ideally.
- The I/O (Input/Output) voltages of the multicellular converter are designed arbitrarily by the number of cell converters connected in ISOP and IPOS.
- The ISOP-IPOS connected multicellular converters using non-regulated DC-DC converters inherently achieve the balanced input voltage sharing and the balanced output current sharing among cell converters without any complicated controls [14].
- The low voltage stress of the cell converter enables to employ the low-voltage and ultra-low loss semiconductor power devices [15].

The high power density DC-DC converter based on the multicellular converter topology has been already reported [7]. However, the magnetic components as the high frequency transformer are generally utilized in the cell converter, and the performance of the cell converter depends on the magnetic components largely. The performance of the magnetic component determined by the material science is one of barriers to achieve high power density converters [11]. The converter circuit topology which reduces the stress of the magnetic components is attractive for future DC distribution systems.

2.2 Multicellular DC-DC Converter Based on Non-isolated Circuit Topology

Fig. 3 shows the circuit configuration of the proposed multicellular DC-DC converter. The proposed converter consists of the non-isolated cell converters and these cell converters are connected in ISOP. The circuit configuration of each cell converter is based on the conventional buck chopper circuit and the bidirectional semiconductor switches Q_k, Q_{xk} in two lines substitute for the single unidirectional transistor in the conventional buck chopper circuit.

The control scheme of the proposed multicellular converter is shown in Fig. 4. The electric power is provided from one of the cell converters (Cell$_k$, k = 1, 2, …, N) to the load by turning on the switches Q_k, Q_{xk} at a certain time, preventing the electrical short circuit among cell converters. Pairs of Q_k, Q_{xk} are turned on alternately as shown in Fig. 4, and the pairs of the bidirectional switches under the turn-off condition make the isolation barrier. The applied voltages to the bidirectional switches Q_k, Q_{xk} are time-variant and these stresses depend on the circuit operating condition.

From Fig. 4, the duty ratio of each cell converter D is limited by the number of cell converters N connected in ISOP. The maximum duty ratio D_{max} is 1/N to prevent the short circuit among cell converters. In the case of D $\leq$ 1/N, the voltage transformation ratio V_{OUT}/V_{IN} is calculated as the following equation, taking the input voltage of the multicellular converter V_{IN} is shared by the cell converters equally into account.

$$\frac{V_{OUT}}{V_{IN}} = \frac{D \cdot V_{ik}}{N \cdot V_{ik}} = \frac{D}{N} \leq D_{max}^2$$

The characteristics of the proposed non-isolated multi-cellular converter are summarized as follows.

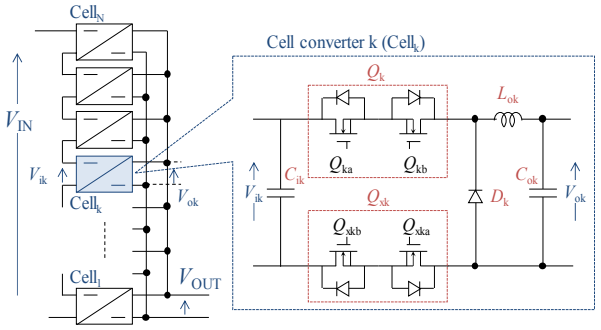

Fig. 3 Configuration of non-isolated DC-DC cell converter using bidirectional semiconductor power switches.

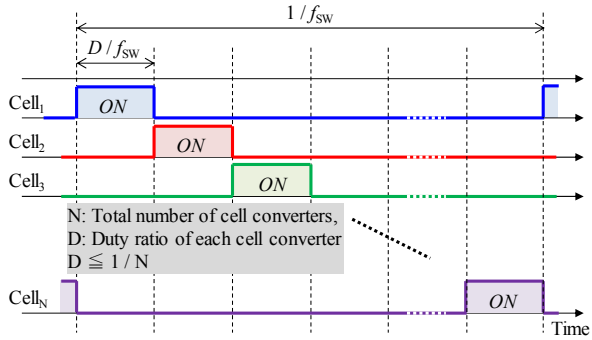

Fig. 4 Control scheme of non-isolated multicellular DC-DC converter.

- The magnetic coupling is not applied. The design for the magnetic components can be simplified under the high frequency operation condition.
- The stress of the magnetic components can be reduced because of the interleaved control among cell converters.
- The proposed converter achieves higher step-down ratio compared with the conventional chopper circuit in the case of the corresponding duty ratio of D. In other word, larger duty ratio is applicable to realize the high step-down converter.
- High speed and ultra-low loss bidirectional devices are indispensable because large numbers of power devices whose rated voltages depend on the input voltage V_{IN} are utilized.

3. Experiment for Non-isolated Multicellular DC-DC Converter

The laboratory prototype has been developed to verify the feasibility of the proposed non-isolated multicellular DC-DC converter. Fig. 5 shows the circuit configuration for the experiment and Fig. 6 shows the experimental apparatus. The multicellular converter consists of two cell converters and these cell converters are connected in ISOP. Each cell converter consists of the main switches Q_k, Q_{xk}, the free-wheeling diode D_k, the input capacitor C_{ik} and the output inductor L_{ok}. The output capacitances for two cell converters are bundled to the capacitance C_{OUT}. Here, the subscript k means the number of the cell converters and k = 1, 2 in this experiment.

The parameters for the experiment are summarized in Table 1. The input voltage of the multicellular converter V_{IN} is 48 V and the prospective output voltage V_{OUT} is 10.8 V because the number of cell converters N is 2 and the duty ratio of each cell converter D is 0.45 (10.8 = 48/2 × 0.45). Si-MOSFETs

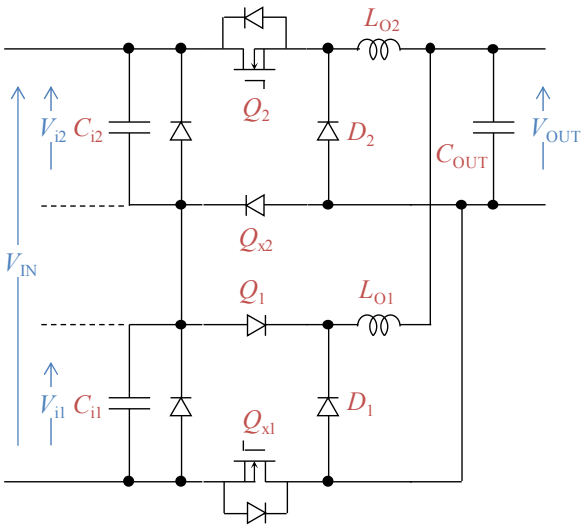

Fig. 5 Circuit configuration of non-isolated multicellular DC-DC converter using two cell converters.

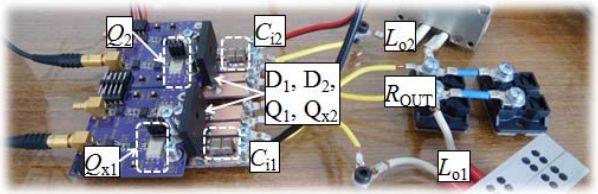

Fig. 6 Experimental apparatus for non-isolated multicellular converter.

Table 1 Parameters for experiment.

Input voltage	V_{IN}	48 V
Output voltage	V_{OUT}	10.8 V
Number of cells	N	2
Duty ratio	D	0.45
Switching frequency	f_{SW}	100 kHz
Main switch	Q_{x1}, Q_2	100 V, 2.8 mΩ (IRF7769 / IR)
Free-wheeling diode, Auxiliary switch	D_k, Q_1, Q_{x2}	200 V, 15 A (D15XBN20 / Shindengen)
Input capacitor	C_{ik}	44 μF, 62 V
Output inductor	L_{ok}	500 μH, 6 A
Resistive load	R_{OUT}	2 Ω (50 W)
Controller		PE—Expert IV (Myway Plus)

k= 1, 2.

(100 V, 2.8 mΩ/IRF7769 from IR) are utilized for the main switch Q_{x1}, Q_2 and Si-SBDs (200 V, 15 A/D15XBN20 from Shindengen) are employed to realize the diode bridges by the pair of Q_1 and D_1 and the pair of Q_{x2} and D_2. In this experiment, the unidirectional transistors and the diodes substituted for the bidirectional semiconductor switches in Fig. 3, because the unidirectional voltage stress is applied to the switches Q_k, Q_{xk} in the case of $N = 2$.

Fig. 7 shows the experimental result of the non-isolated multicellular DC-DC converter using two cell converters. The input voltage of the multicellular converter V_{IN} was 48 V and the input voltages of cell converters V_{i1}, V_{i2} were 24 V, respectively. This means the input voltage of the multicellular converter

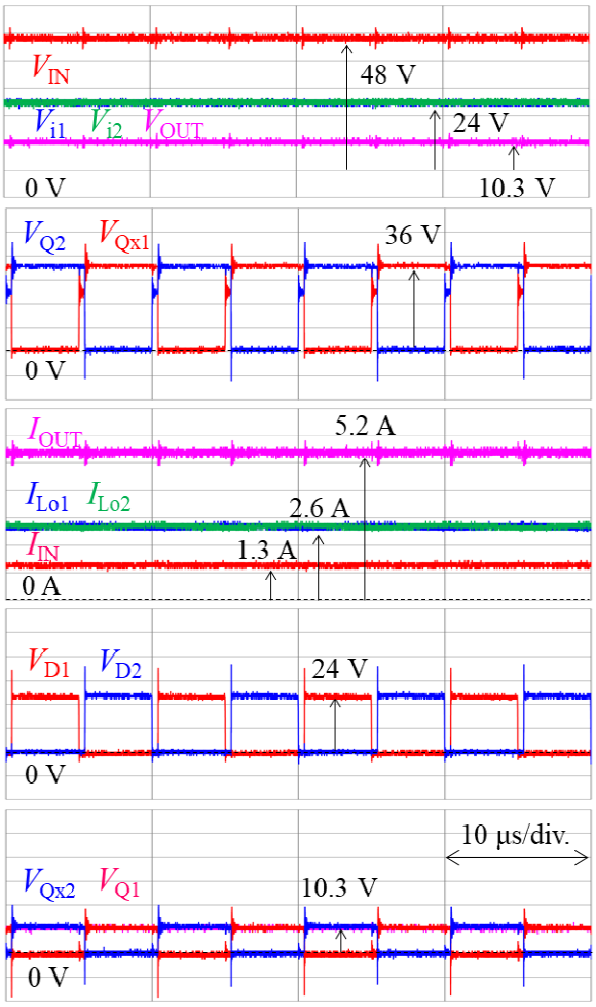

Fig. 7 Experimental result for non-isolated multicellular converter.

was shared equally by the series connected two cell converters. The output voltage V_{OUT} was 10.3 V. The measured output voltage was lower than the prospective output voltage of 10.8 V because of the forward voltage drops of the diodes Q_1, Q_{x2}, D_1, and D_2 mainly. From this experiment, the efficiency of the converter was estimated at 95.4% (= 10.3 V/10.8 V) under the resistive load of 2 Ohms.

The symbols of V_{Qx1}, V_{Q2} mean the drain to source voltage of Si-MOSFETs. The applied voltages to the main switches were higher than the input cell voltages V_{i1}, V_{i2} of 24 V because the input DC voltage V_{IN} was blocked by the main switches under the turn-off state. The output current I_{OUT} was 5.2 A and this output current was total amount of the inductor current I_{Lo1}, I_{Lo2}. Because two cell converters deliver the electric power to the load alternately as shown in V_{Qx1}, V_{Q2} of Fig. 7, the interleaved waveforms were observed in the inductor currents.

The voltages of the free-wheeling diodes V_{D1}, V_{D2} were also shown in Fig. 7. The applied voltages to the V_{D1}, V_{D2} correspond to the input cell voltages V_{i1}, V_{i2}. This result means that the multicellular converter topology contributes to reducing the voltage stresses for the free-wheeling diodes and the passive components.

The amplitude of the applied voltages to the power devices Q_1, Q_{x2} were 10.3 V from Fig. 7. Difference between Q_k and Q_{xk} ($k = 1, 2$) corresponds to the input cell voltage V_{ik} and the total amount of Q_k and Q_{xk} means the blocking voltage for the isolation barrier.

Fig. 8 shows the simulation result using PSIM software. The circuit configuration and the circuit parameters correspond to the circuit in Fig. 5 and the parameters in Table 1 respectively. The characteristics of the on-resistance and the forward voltage drop of the semiconductor power devices Q_k, Q_{xk}, D_k were not taken into account and the constant values obtained from the published datasheet for the equivalent capacitances were applied to the junction capacitance of Q_k, Q_{xk}, D_k. The simulation result had good agreement

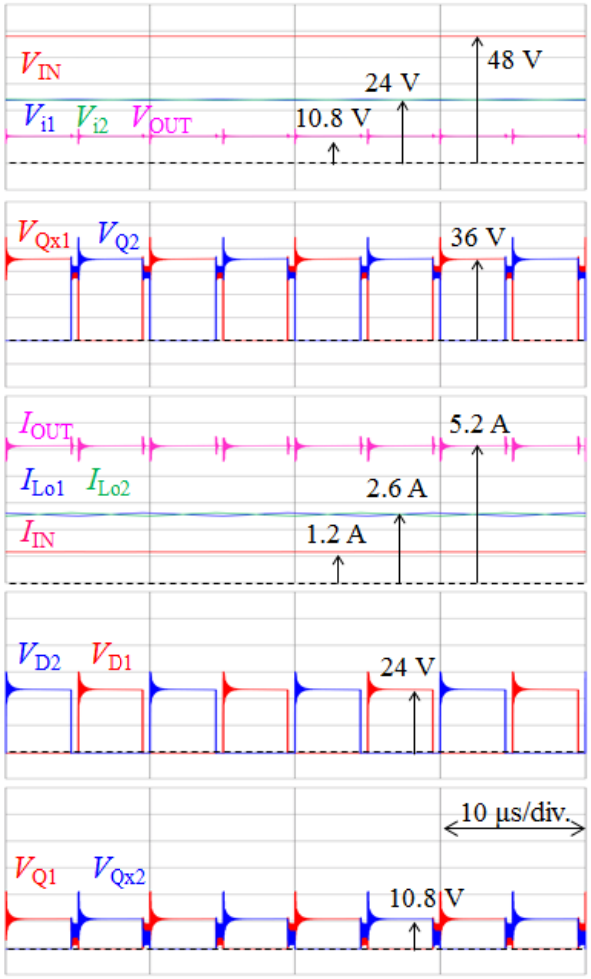

Fig. 8 Simulation result for non-isolated multicellular converter.

with the experimental result. This means that the behavior of the non-isolated multicellular converter using N cell converters is predicted exactly.

4. Design Consideration for Highly Efficient Multicellular DC-DC Converter

Design consideration for 48 V-3 V, 210 W non-isolated multicellular DC-DC converters is conducted here. The circuit configuration is shown in Fig. 9 and four cell converters are connected in ISOP. The rated I/O voltages of each cell converter are 12 V and 3 V respectively, and each cell converter is driven by the duty ratio D of 0.25. Here, the transistors Q_{SRk} (k = 1, …, 4) substituted for the free-wheeling diodes to reduce the conduction loss by the synchronous rectification.

Parameters for this design are shown in Table 2. The breakdown voltage of the bidirectional main switch is based on the total input voltage V_{IN} for the isolation barrier, and the GaN-FETs (100 V, 7 mΩ) were assumed for the main switches here. The GaN-FETs (30 V, 1.3 mΩ) were assumed for the transistors Q_{SRk} (k = 1, …, 4) to achieve the synchronous rectification. The design for the output inductors L_{ok}, the input capacitors C_{ik} and the output capacitors C_{ok} are based on the conventional 12 V-3 V, 52.5 W (= 210 W/4) buck chopper circuit. The passive components L_{ok}, C_{ik}, C_{ok} are determined to suppress the current ripple within 20% and the voltage ripple within 3% under the condition that the switching frequency varied from 100 kHz to 1 MHz.

Fig. 10 shows the simulation result of the non-isolated multicellular 48 V-3 V converter in case that the bidirectional switches Q_k, Q_{xk} (k = 1, 2, 3, 4) were driven at the switching frequency of 100 kHz. The total input voltage V_{IN} of 48 V is shared by four cell converters and the output voltage V_{OUT} of 3 V was applied to the load. The output inductor currents I_{Lok}

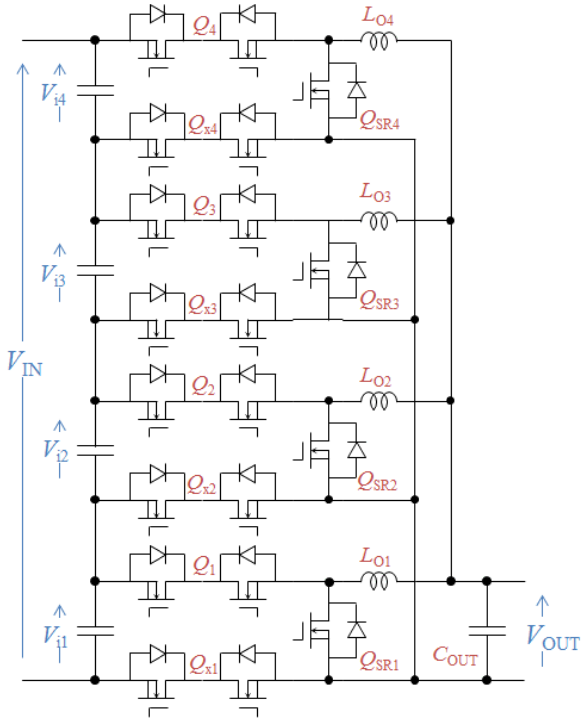

Fig. 9 Circuit configuration of multicellular DC-DC converter using four cell converters.

Table 2 Parameters for design.

Input voltage	V_{IN}	48 V
Input cell voltage	V_{ik}	12 V
Output voltage	V_{OUT}	3 V
Output power	P_{OUT}	210 W
Number of cells	N	4
Duty ratio	D	0.25
Switching frequency	f_{SW}	100 kHz to 1 MHz
Main switch	Q_k, Q_{xk}	100 V, 7 mΩ (EPC2001C/EPC)
Synchronous rectifier	Q_{SRk}	30 V, 1.3mΩ (EPC2023/EPC)
Output inductor	L_{ok}	Ripple 17.5 A ± 20% (SER, SLC/Coilcraft)
Input capacitor	C_{ik}	Ripple 12 V ± 1.5% (MLCC/TDK)
Output capacitor	C_{OUT}	Ripple 3 V ± 1.5% (MLCC/TDK)

k = 1, 2, 3, 4.

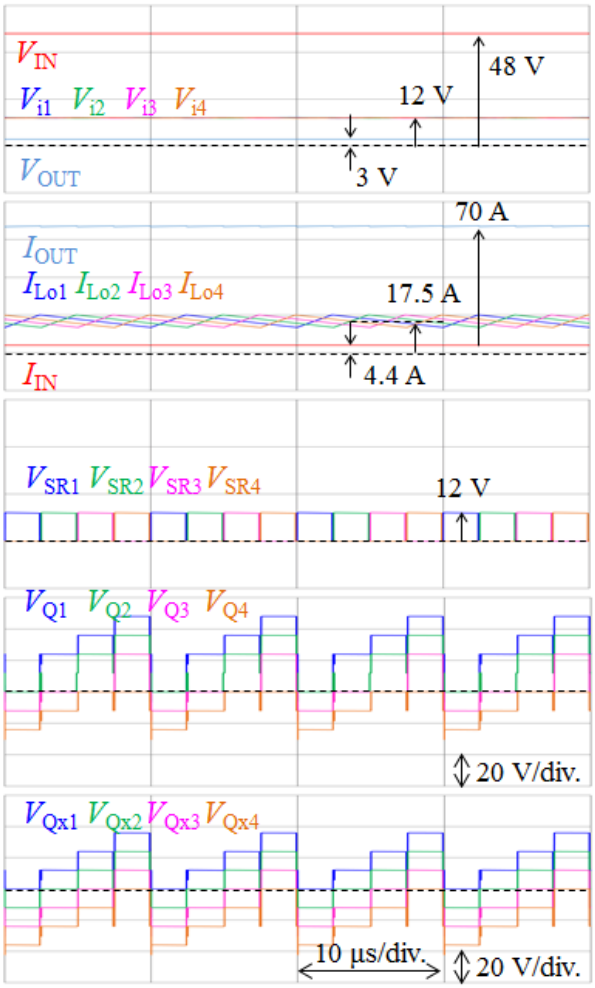

Fig. 10 Simulation result for 48 V-3 V non-isolated multicellular converter using four cell converters.

were balanced and the low ripple output current I_{OUT} was obtained because of the interleaved control. The applied voltage to the bidirectional switches V_{Qk}, V_{Qxk} were also shown in Fig. 10. The turn-on loss energies generated from the bidirectional switches can be estimated from the simulation result. In this simulation, the influence of the parasitic parameters was not considered to confirm the fundamental behavior of the proposed circuit.

The calculation result of the converter loss was shown in Fig. 11. The conduction loss $P_{con(Q)}$, the switching loss $P_{sw(Q)}$ were considered for the bidirectional switch Q_k, Q_{xk} (k = 1, …, 4). The power loss limit model for the high-speed ultra-low loss power devices was applied to estimate the switching loss, and the minimum switching loss caused by the stored energy in the junction capacitance was calculated [16, 17]. The copper loss $P_{cu(Lo)}$ and the core loss $P_{core(Lo)}$ were also considered for the output inductor L_{ok} (k = 1, …, 4), and these losses were estimated by using the published datasheet and the design tool provided from the manufacturer. The power losses generated from the capacitors were not considered here. As shown in Fig. 11, the conduction losses generated from the bidirectional switches were dominant because of the numerical quantity of the bidirectional switch whose voltage stress depends on the input voltage V_{IN} for the isolation barrier. To accomplish higher efficiency, lower on-resistance of the transistors for the bidirectional switch and the novel

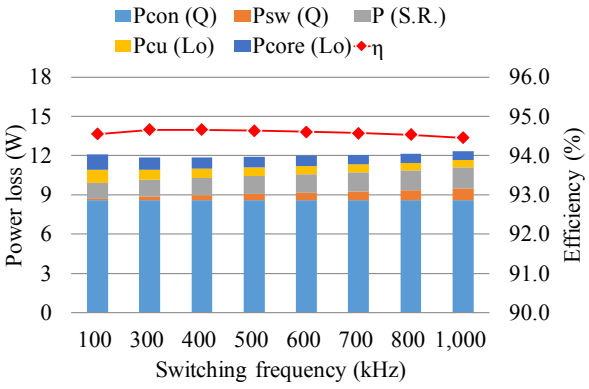

Fig. 11 Estimated power loss and conversion efficiency.

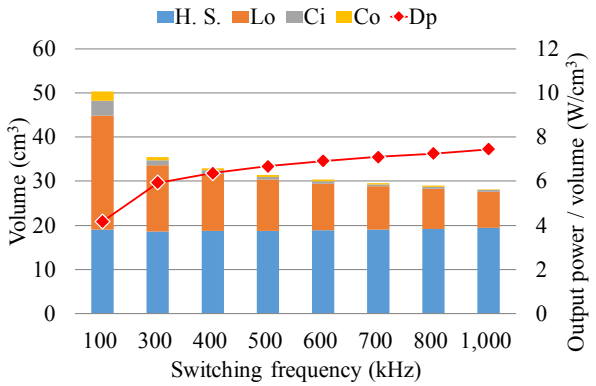

Fig. 12 Estimated converter volume and power density.

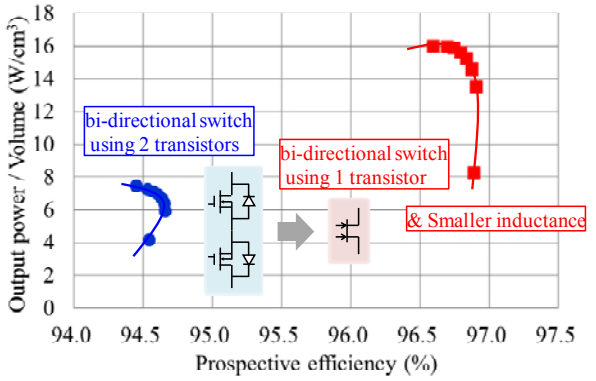

Fig. 13 Estimated conversion efficiency and power density.

power device configuration to realize the bidirectional switch by using the single transistor is indispensable [18].

The estimated converter volume was shown in Fig. 12. Volumes for the output inductor *Vol*(L_{ok}), the inputcapacitor *Vol*(C_{ik}) and the output capacitor *Vol*(C_{OUT}) were considered. The heat sink volume was also simply estimated under the condition that the heat dissipation efficiency was 0.65 W/cm^3 [19, 20]. The volume for the heat sink was approximately constant in case that the switching frequency varied from 100 kHz to 1 MHz because of the dominant conduction loss in Fig. 11. The inductor volume was influential on the power density and the higher switching frequency operation contributes to realizing the higher power density converter. Larger current ripple for the output inductor contributes to minimizing the inductor volume, taking the effect of the interleaved control into account.

Fig. 13 shows the prospective conversion efficiency and the output power density of the proposed multicellular converter. The bidirectional switch was assumed to be developed by the single power device. The output inductor was designed to achieve the BCM (boundary current mode) for minimizing the inductor volume. The performances for the power dissipation and the converter volume were improved and the efficiency approaches the designated 97% in Fig. 1.

5. Conclusions

The non-isolated multicellular DC-DC converter was newly proposed for highly efficient high step-down POL converters in the next generation DC distribution system. The circuit configuration, the control scheme and the characteristics of the proposed converter were briefly introduced. The 48 V multicellular converter using two cell converters connected in ISOP was developed and the feasibility of the proposed converter was confirmed experimentally. Design consideration for the 48 V-3 V multicellular converter using four cell converters was carried out, and the potential for higher efficiency and higher power density was shown. The proposed multicellular converter contributes to the energy—saving of the DC distribution system for future low carbon society.

References

[1] Ministry of Internal Affairs and Communications. 2015. "WHITE PAPER Information and Communications in Japan."

[2] Schmidt, R. R., Belady, C., Classen, A., Davidson, T., Herrlin, M. K., Novotny, S., and Perry, R. 2004. "Evolution of Data Center Environmental Guidelines." *ASHRAE Transactions* 110 (1): 559-66.

[3] Sugiyama, Y. 2011. "Green ICT toward Low Carbon Society." Design for Innovative Value towards a Sustainable Society. In *Proceedings of the Eco. Design 2011, 7th International Symposium on Environmentally Conscious Design and Inverse Manufacturing*, 739-42.

[4] Ninomiya, T., Ishizuka, Y., Shibahara R., and Abe, S. 2012. "Energy-Saving Technology Using Next-Generation Power Electronics." In *Proceedings of the IEE-Japan Industry Applications Society Conference,* I 15-20.

[5] Babasaki, T., Tanaka, T., Nozaki, Y., Tanaka, T., Aoki T., and Kurokawa, F. 2009. "Developing of Higher Voltage Direct-Current Power-Feeding Prototype System." In *Proceedings of the International Tele-communications Energy Conference (INTELEC*), 1-5.

[6] Zhou, L., Wu, Y., Honea J., and Wang, Z. 2015. "High-Efficiency True Bridgeless Totem Pole PFC Based on GaN HEMT: Design Challenges and Cost-Effective Solution." In *Proceedings of PCIM Europe, Nuremberg, Germany*.

[7] Hayashi, Y. 2013. "High Power Density Rectifier for Highly Efficient Future DC Distribution System." *Journal of Electrical Engineering Research, Electrical Engineering Publishing Company* 1 (3): 49-59.

[8] Ahmed, M., Fei, C., Lee, F. C., and Li, Q. 2017. "High-Efficiency High-Power-Density 48/1 V Sigma Converter Voltage Regulator Module." In *Proceedings of Applied Power Electronics Conference and Exposition (APEC)*, 2207-12.

[9] Hwu, K. I., Jiang, W. Z., and Yau, Y. T. 2016. "Nonisolated Coupled-Inductor-based High Step-down Converter with Zero DC Magnetizing Inductance Current and Nonpulsating Output Current." *IEEE Transactions on Power Electronics* 31 (6): 4362-77.

[10] Zhao, X., Yeh, C., Zhang, S. L., and Lai, J. S. 2017. "A High-Frequency High-Step-down Converter with Coupled Inductor for Low Power Applications." In *Proceedings of Applied Power Electronics Conference and Exposition (APEC),* 2436-40.

[11] Kolar, J. W. 2014. "What Are the Big Challenges in Power Electronics?" Presented at 8th International Conference on Integrated Power Electronics Systems (CIPS).

[12] Strydom, J., and White, B. 2010. "High Step-down Ratio Buck Converters with eGaN Devices." *How2power* 1-15.

[13] http://www.vicorpower.com/.

[14] Hayashi, Y., and Ninomiya, T. 2016. "Analysis and Prototyping of Multicellular DC-DC Transformer for Environmentally Friendly Data Centers." *Journal of Energy and Power Engineering* 10 (5): 313-23.

[15] Tolbert, L. M., Ozpineci, B., Islam, S. K., and Chinthavali, M. S. 2003. "Wide Bandgap Semiconductors for Utility Applications." In *Proceedings of the International Association of Science and Technology for Development (IASTED) International Conference on Power and Energy Systems (PES)*, 317-21.

[16] Nakajima, A., Takao, K., and Ohashi, H. 2013. "GaN Power Transistor Modeling for High-Speed Converter Circuit Design." *IEEE Transactions on Electron Devices* 60 (2): 646-52.

[17] Takao, K., and Ohashi, H. 2013. "Accurate Power Circuit Loss Estimation Method for Power Converters with Si-IGBT and SiC-Diode Hybrid Pair." *IEEE Transactions on Electron Devices* 60 (2): 606-12.

[18] Morita, T., Yanagihara, M., Ishida, H., Hikita, M., Kaibara, K., Matsuo, H., Uemoto, Y., Tanaka, T., and Ueda, D. 2007. "650 V 3.1 $m\Omega/cm^2$ GaN-based Monolithic Bidirectional Switch Using Normally-off Gate Injection Transistor." In *Proceedings of IEEE International Device Meeting*, 865-8.

[19] Tsukuda, M., Omura, I., Domon, T., Saito, W., and Ogura, T. 2005. "Demonstration of High Output Power Density (30 W/cc) Converter Using 600 V SiC-SBD and Low Impedance Gate Driver." In *Proceedings of the 2005 International Power Electronics Conference (IPEC)*, 1184-9.

[20] Hayashi, Y., and Mino, M. 2014. "An Approach to a Higher-Power-Density Power Supply for a 380-V DC Distribution System." *Electrical Engineering in Japan* 186 (3): 51-62.